IEEE Access
Multidisciplinary | Rapid Review | Open Access Journal

Received September 21, 2017, accepted October 11, 2017, date of publication October 16, 2017,
date of current version November 14, 2017.

Digital Object Identifier 10.1109/ACCESS.2017.2763177

A Wideband Base Station Antenna Element With Stable Radiation Pattern and Reduced Beam Squint

HAIHAN SUN, (Graduate Student Member, IEEE), CAN DING, (Member, IEEE), BEVAN JONES, (Life Member, IEEE), AND Y. JAY GUO, (Fellow, IEEE)
Global Big Data Technologies Centre, University of Technology Sydney, Ultimo, NSW 2007, Australia
Corresponding author: Can Ding (can.ding.1989@gmail.com)

This work was supported by the Australian Research Council under Grant DP160102219.

ABSTRACT This paper presents the design procedure, optimization strategy, theoretical analysis, and experimental results of a wideband dual-polarized base station antenna element with superior performance. The proposed antenna element consists of four electric folded dipoles arranged in an octagon shape that are excited simultaneously for each polarization. It provides ±45° slant-polarized radiation that meets all the requirements for base station antenna elements, including stable radiation patterns, low cross polarization level, high port-to-port isolation, and excellent matching across the wide band. The problem of beam squint for beam-tilted arrays is discussed and it is found that the geometry of this element serves to reduce beam squint. Experimental results show that this element has a wide bandwidth of 46.4% from 1.69 to 2.71 GHz with ≥15-dB return loss and 9.8 ± 0.9-dBi gain. Across this wide band, the variations of the half-power-beamwidths of the two polarizations are all within 66.5° ± 5.5°, the port-to-port isolation is >28 dB, the cross-polarization discrimination is >25 dB, and most importantly, the beam squint is <4° with a maximum 10° down-tilt.

INDEX TERMS Base station antenna element, dual-polarization, stable radiation patterns, beam squints.

I. INTRODUCTION

The environmental demands and the rising costs of acquiring new sites for base stations along with the need for increased capacity of mobile networks have led to ever more stringent requirements on base station antennas. In particular, there has been a strong demand in combining high and low band antennas into a single package sharing a common ground plane. In such antennas, certain techniques that are suitable for single band antennas such as surrounding radiating elements with metal walls or shaping the ground plane are generally unacceptable. On the other hand, high performance such as wide bandwidth, high port-to-port isolation, great cross-polarization discrimination (XPD), beamwidth consistency, and little beam squint needs to be preserved as much as possible. There are many challenges in meeting all these specifications simultaneously. As a result, there has been increasing research activities in base station antennas recently [1]–[20].

Among all the base station antenna elements employed in the mobile industry, the cross-dipole is the most commonly used antenna element. Cross-dipole antennas can be generally classified into two types. Type-I employs two electric dipoles placed perpendicular to each other [1]–[12], and type-II utilizes four dipoles consisting of two pairs of magneto-electric dipoles (ME-dipoles) [13]–[15]. For the type-I cross-dipole antennas, broad impedance bandwidths with excellent matching can be achieved by utilizing strong mutual coupling between the two electric dipoles [1]–[8], adding parasitic radiator and director [1], or using multimode radiators [2], [3]. Most of them can fulfill the requirements for the base station antenna elements, and their performances are preserved in the corresponding base station antenna arrays [9]–[11]. However, their radiation patterns intrinsically vary significantly across a wide band [4], as the patterns are mainly due to the radiation of one dipole for each polarization. In order to stabilize the radiation pattern, shaped ground or walls [1]–[3], [5]–[11] are employed. These techniques are suitable for single band antennas but they may cause undesirable scattering in the other band in dual band antenna systems and therefore should be avoided. Moreover, adding walls increases the size, weight, and cost of the antennas. This problem will add complexity when the antenna

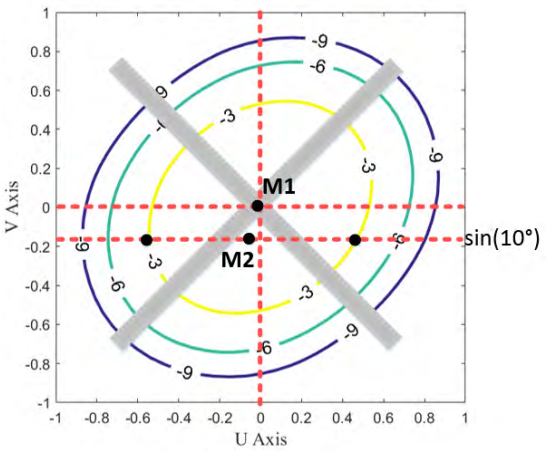

FIGURE 1. Contour of the normalized radiation pattern of a cross-dipole placed above a ground plane.

element is applied in a 5G massive MIMO system consisting of a large number of antenna elements. Instead of using walls, type-II ME-dipoles, can achieve relatively stable radiations by introducing additional magnetic dipoles [13], [14]. In [14], a dual-polarized, low-profile ME-dipole antenna element with dielectric loading is proposed. It has very stable radiation patterns, but its bandwidth is only 24.9% with $|S_{11}| < -10$ dB. The bandwidth of the ME-dipole is enhanced to 50% with excellent matching in [15], but its radiation patterns vary greatly within the operation band. Therefore, it still seems to be a challenge for ME-dipoles to achieve excellent matching and stable radiation patterns at the same time. In addition to the aforementioned cross-dipole configurations, there is another type of configuration with four end-to-end electric dipoles forming a square loop (type-III square dipole array) [16]–[20], which also has the potential to fulfill the specifications of the base station antenna element. The four electric dipoles are excited simultaneously for each polarization, and ±45° polarizations are achieved by utilizing two different feed networks. Beam consistency has been achieved with half-power beamwidth (HPBW) variation <10°, but the bandwidth is limited (<30%) in the reported works [18]–[20]. Moreover, there has been no report on the working mechanism of such antennas. Without the insight of how this type of antennas works, it would be difficult to improve its performance.

Beam squint is an important parameter for the down-tilted base station antenna arrays but it has rarely been discussed in the open literature. It is a parameter that measures the difference between the mechanical boresight and the horizontal beam pointing angle of the antenna, representing the symmetry of the main beam. Elliptical beamshape of array elements is the main source of squint. For a simple dipole, it has the characteristic that the beamwidth in the E-plane is substantially narrower than that in the H-plane. When used in an array, this leads to problems of unbalanced grating lobes and squint when the beam is tilted. As an example, Fig. 1 shows a coutour plot of the radiation pattern of a typical type-I

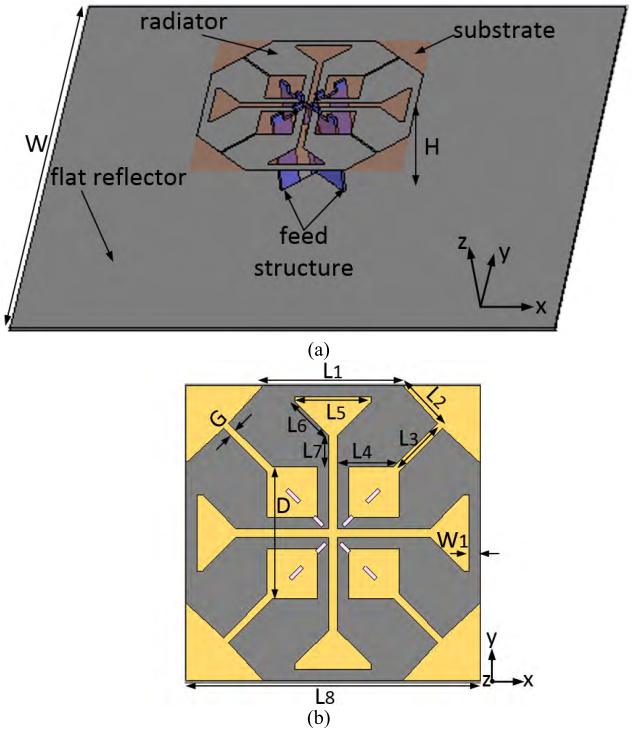

FIGURE 2. (a) Perspective view of the proposed antenna. (b) Top view of the aperture.

cross-dipole in u-v (direction cosine) coordinates. Without down-tilt, the beam peak (M1) is in the direction of the mechanical boresight. With a down-tilt angle of 10°, the beam peak (M2) shifts away from the mechanical boresight, thus resulting in squint. The beam of the orthogonal polarization moves in the opposite direction which leads to different coverage for the two polarizations and a degradation in MIMO performance. In the celluar industry, the beam squint of base station antenna array is typically required to be less than 5° for a down-tilt range from 0° to 10°.

In this paper, a dual-polarized antenna comprising four folded dipoles with superior performance that meets all the specifications of 4G base station antenna elements is proposed. Theoretical analysis is carried out based on the current distribution to obtain insight and to provide qualitative explanations to the achieved performance. The currents on the folded dipoles are more symmetrically distributed than those on a typical cross-dipole, so that the resultant beam is almost circularly symmetric. Having a circularly symmetric beam prevents the beam squint problem when the antenna element is used in a down-tilted array.

In this paper, we firstly present the configuration of the proposed antenna element employing four folded dipoles, and analyze their combined radiation patterns. Based on the analysis, the dimensions of the folded dipoles are determined to achieve desired HPBW with good beam consistency and reduced beam squint. Subsequently, unique feed networks for the two polarizations are designed based on a circuit theory model and then implemented using microstrip lines. Finally, experimental results of the optimized and

TABLE 1. Optimized parameters of the radiator.

Parameter	W	H	L_1	L_2	L_3	L_4	L_5
Value (mm)	200.00	27.00	33.48	12.73	14.76	14.22	18.36
Parameter	L_6	L_7	L_8	G	W_1	D	
Value (mm)	11.39	7.56	70.38	0.64	2.70	31.50	

well-matched antenna element are presented, which are in good agreement with simulation results.

II. ANTENNA CONFIGURATION

The configuration of the broadband dual-polarized antenna element is shown in Fig. 2. It consists of four folded dipole radiators, two microstrip feed structures, and a flat square metallic plate as reflector. The four folded dipoles are printed on an FR4 substrate and are closely arranged in the shape of an octagon. The folded dipole arms are fed by parallel lines to four points forming a square at the center of the board. They are excited by two feed structures in the diagonal directions to realize the ±45° polarizations. When one polarization is excited, all four folded dipoles are used and are excited in two pairs of series connected dipoles. The two feed structures are mounted between the radiator and the reflector. The details of the feed structure are discussed in Section III. The distance between the radiator and the reflector is 27 mm, which is 0.20λ at 2.2 GHz. All the substrates employed in Fig. 2 are FR4 substrate with a dielectric constant of 4.3 and loss tangent of 0.02. The thicknesses of substrate for the radiator and feed structures are 0.5 mm and 1.0 mm, respectively. The optimized parameters of the radiator are listed in Table 1.

III. WORKING PRINCIPLE ANALYSIS

A. HALF-POWER BEAMWIDTH

To understand the working principle of the proposed antenna, we examined the current distribution on four folded dipoles arranged in an octagon, as shown in Fig. 3(a). The parallel conductor transmission lines carry principally balanced currents and make a very minor contribution to the radiation pattern, therefore they are not considered in the analysis. All the four dipoles are excited simultaneously to realize the ±45° polarizations. Fig. 3(a) shows the ideal excitation method to achieve the −45° polarization as an illustration, where four 50-Ohm discrete ports are added across the edge of the four folded dipoles and all the four ports are excited simultaneously. The arrows represent the direction of the excitations. The resultant current distribution at 2.2 GHz in this case is shown in Fig. 3(b). It is clear that dipoles I and II radiate horizontal polarization (HP) while dipoles III and IV radiate vertical polarization (VP). We can separate these two components and calculate their beams in the horizontal plane (*xoz*-plane). The finite ground plane has different and quite significant effects on the HP and VP beamwidths. To separate the variation caused by the element from the variation caused by the width of the ground plane, we firstly examine the case of an infinite ground plane.

The simulated variations of VP and HP HPBWs with frequency are shown in Fig. 4(a) for the case of an infinite

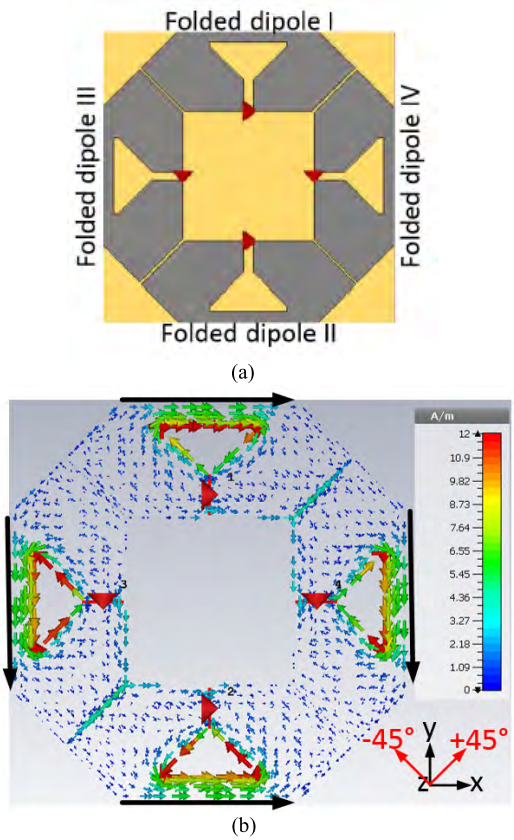

FIGURE 3. (a) Configuration of the radiator without feed network. (b) Current distribution on the radiator at 2.2 GHz.

ground plane. It is seen that the variation of the HPBWs of the −45° co-polar combination is <5° across the band. To understand the factors influencing this variation, we compared this plot with the HPBW variations of four simple linear dipoles with sinusoidal current distributions, as shown in Fig. 4(b). The substitute linear dipoles are aligned with the centers of the actual folded dipoles.

The factors affecting the beams in the horizontal plane are:

- Horizontal polarization

a) Dipole pattern

$$f_{hd} = [cos(k\frac{l}{2}\cos\alpha) - \cos(k\frac{l}{2})]/\sin\alpha \qquad (1)$$

where l is the effective length of the dipole, $k = \frac{2\pi}{\lambda}$ is the wave factor, and α is the azimuth angle in the horizontal plane [21].

b) Height above ground plane

$$f_{gp} = \sin(kH\cos\alpha)/\sin(kH) \qquad (2)$$

where H is the height of the dipoles above the ground plane. This is calculated based on the pattern of a source and its image in the infinite ground plane.

- Vertical polarization

a) Pattern of pair of vertical dipoles in the horizontal plane

$$f_{vd} = \cos(k\frac{s}{2}\sin\alpha) \qquad (3)$$

where s is the horizontal spacing of the dipoles.

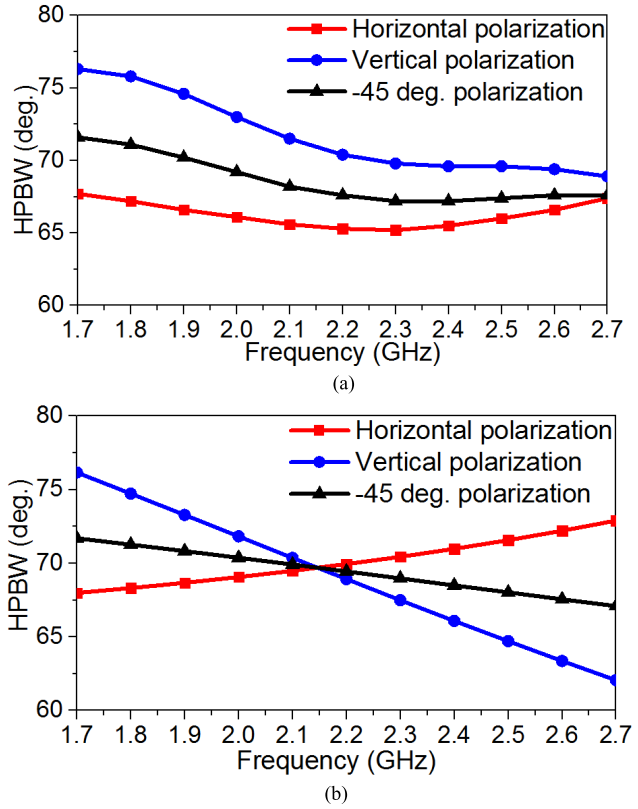

FIGURE 4. **(a) The simulated and (b) the calculated HPBW variations of HP, VP, −45° -polarized patterns of the element in the horizontal plane with an infinite ground plane.**

b) Height above ground plane

$$f_{gp} = \sin(kh\cos\alpha)/\sin(kh) \tag{4}$$

The HP and VP beams in the horizontal plane are given by $f_{hd} \times f_{gp}$ and $f_{vd} \times f_{gp}$, respectively. The HPBWs of these patterns along with the HPBWs of the −45° co-polar combination of the orthogonal polarizations are plotted in Fig. 4(b). The parameters used in this calculation were height H = 27mm (actual value), dipole length L = 51.5mm (end to end length of folded dipole), and dipole spacing s = 52.4 mm (spacing of centerlines of the folded dipoles). The agreement with the simulation results of Fig. 4(a) is quite close in values, although the curvature is not predicted by the elementary model. This discrepancy must be attributed to variation of the current distribution with frequency on the wide folded dipoles. Both plots show a relatively stable −45° co-polar HPBW with a total variation of approximately 5° across the band.

As discussed above, dipole length (L), dipole separation distance (D), and antenna height (H) have noticeable effects on the radiation patterns. Here we remark that infinite ground plane was considered in (1) to (4), however, the finite reflector size (W) in the practical application has great influence on the radiation pattern as well. The effects of D, H, and W on the HPBWs are illustrated in Fig. 5. Note that the influence of dipole dimensions is not considered as it is a dominate parameter for impedance matching.

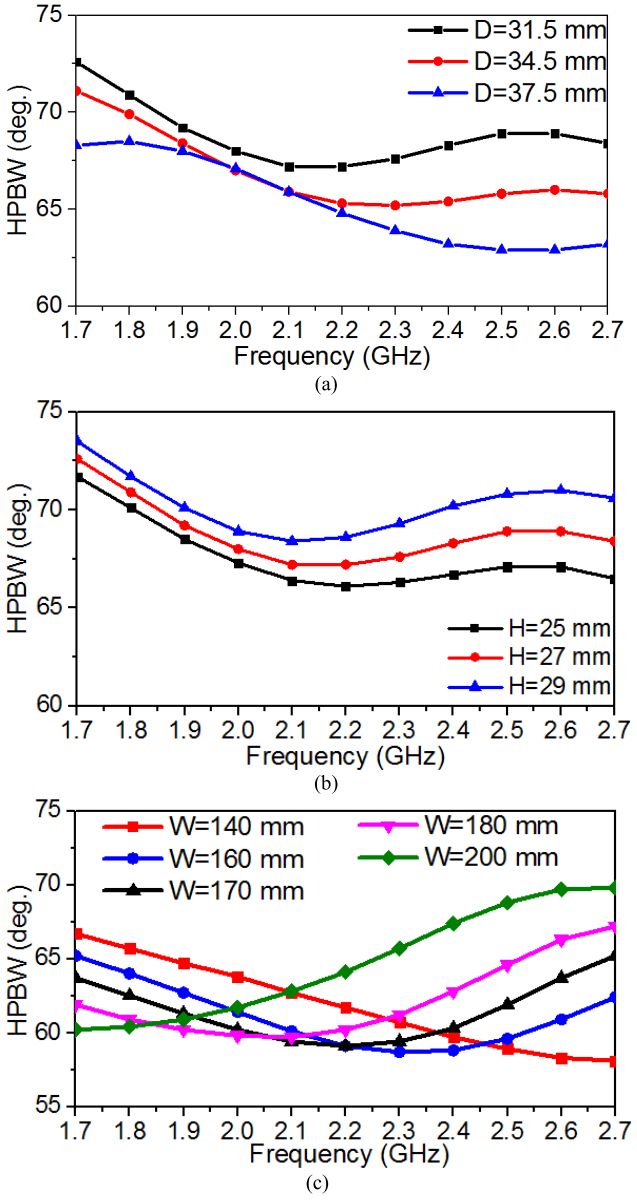

FIGURE 5. **Variation of co-polar HPBWs across the band with (a) different distance *D* between the folded dipole elements, (b) different antenna height *H*, and (c) different widths *W* of ground plane.**

As shown in Fig. 5(a) and (b), the HPBW gets narrower with an increasing distance between the folded dipoles (D) or with a decreasing antenna height (H). The pattern variations attributed to these two parameters are moderate and can be used for fine tuning. As observed in Fig. 5 (c), while there is a significant variation in HPBWs caused by the width of the ground plane, selection of an optimum width of ground plane about 170 mm again results in a total variation in HPBW of about 5°. The HPBWs of the VP, HP, and −45° co-polar combination of the orthogonal polarizations for this optimum configuration are shown in Fig. 6.

B. BEAM SQUINT

A characteristic of slant polarized arrays is that they show squint when the beam is tilted away from horizontal plane if

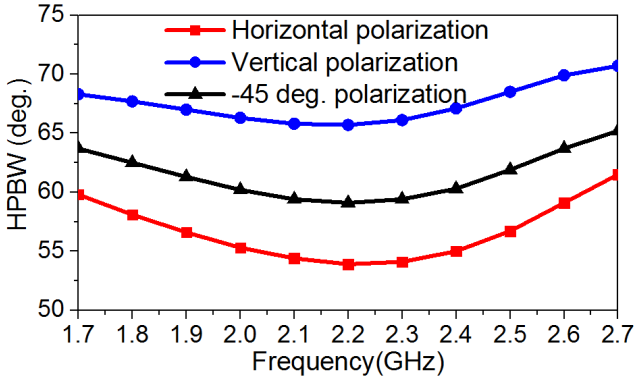

FIGURE 6. HP, VP and co-polar HPBWs of the antenna element placed on a ground plane of width 170 mm.

the E- and H-plane beamwidths of the radiating patterns are unequal. The long axis of the intrinsically elliptical pattern of a conventional 45° -inclined dipole element is aligned 45° away from the y-axis, which destroys the symmetry with respect to the y-axis. Therefore, with a down-tilt angle, the peak of the cut of interest no longer stays at the mechanical boresight, as shown in Fig. 1. To alleviate the beam squint problem, the solution is to make the intrinsically elliptical pattern as circular as possible. To evaluate the severity of the beam squint, a factor is defined as $n = \text{HPBW}(+45°)/\text{HPBW}(-45°)$, which represents the ratio of HPBW in the $+45°$ plane to that in the $-45°$ plane. The closer the value n to 1, the less the squint will be. Here we remark that beam squint of an antenna element is approximately equal to that of the array employing the antenna elements.

To eliminate the beam squint, the E- and H- plane patterns of the element need to be equal in beamwidth. With a pair of crossed dipoles shown in Fig. 7(a), when $-45°$ polarization is excited, a line current is induced along y'-axis. This leads to a narrow E-plane pattern and a broad H-plane pattern, as shown in Fig. 7 (c). Widening the induced currents along x'-axis can help to achieve similar radiation patterns in the two planes. Square patch antennas give rise to much less squint than normal dipole antennas, however, typically their bandwidth is inadequate. In the element described here, the current of a single dipole is replaced by the currents in all four dipoles, and the current distribution is illustrated in Fig. 7(b). The extent of the currents along *x'-axis* is broadened, making the H-plane patterns narrower while maintain the E-plane pattern almost unchanged, as shown in Fig. 7(d). For the cross-dipole model as shown in Fig. 1, $n = 1.29$ at its resonant frequency. For the element described in this paper, n varies from 1.09 to 1.20 across the entire targeted band, demonstrating its ability to suppress beam squint.

IV. FEED NETWORK

In order to excite the four dipoles simultaneously for each polarization, the configuration in Fig. 8(a) is used. Parallel conductor transmission lines connect each folded dipole to the feed points AB and CD as shown in the diagram. If signal is fed in across AB, it is applied to a series connection of

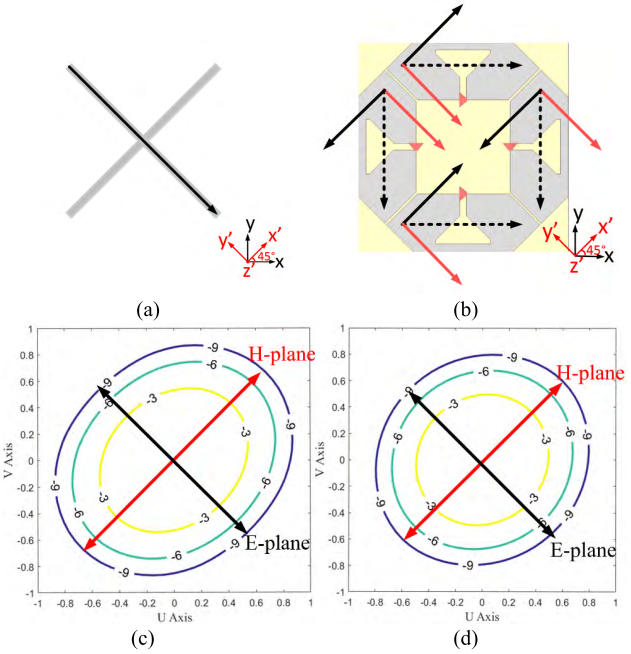

FIGURE 7. Current distribution illustration of (a) a cross-dipole, and (b) the four folded dipole elements; contour plot of beam of (c) a cross-dipole, and (d) the four folded dipole elements in *u-v* coordinates.

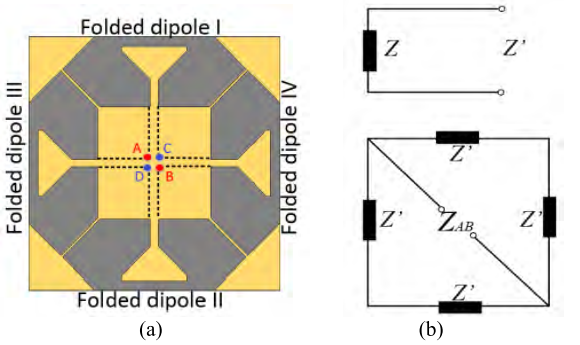

FIGURE 8. (a) Feed method and (b) the equivalent circuit model of the impedance.

the impedances of dipole I and dipole IV each seen through the length of transmission line. Connected in parallel with this combination is the series connection of dipoles II and III each seen through the length of transmission line. Each dipole has the same impedance Z which is transformed to Z' through the lengths of parallel conductor line. Across the feed points AB (or CD) we see two impedances of 2Z' in parallel. The impedance seen at AB or CD is therefore Z'. Matching the input impedance at AB is therefore equivalent to matching the input impedance of each folded dipole with the associated section of transmission line. Therefore, firstly we need to optimize each folded dipole to get readily matched input impedance while maintaining the desired radiation performance.

There are four factors that have great influences on the input impedance: gap width between the folded dipoles (G), antenna height (H), outer perimeter (OP) of the folded dipoles where $OP = L_1 + 2 \times L_2 + 2 \times L_3 + 2 \times L_4$, and inner perimeter ($IP$) of the folded dipoles where

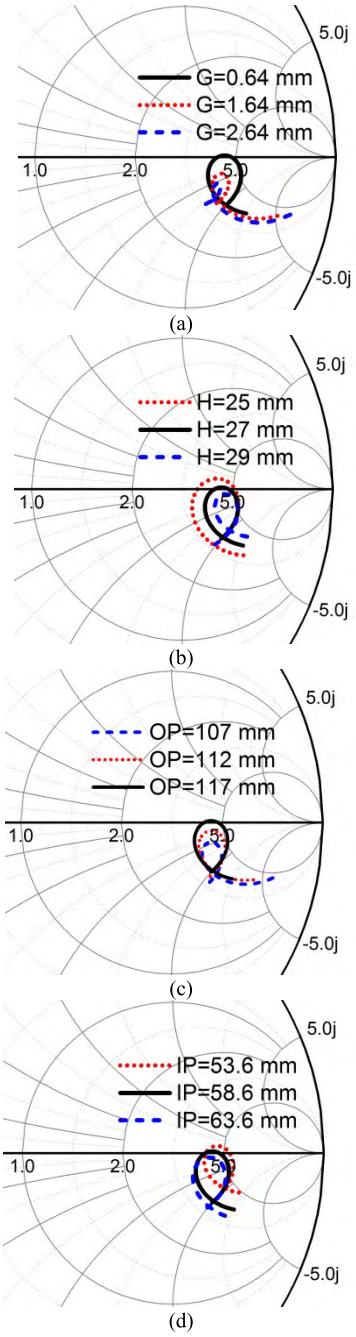

FIGURE 9. Input impedance of the folded dipole elements (Z) on the Z-Smith for parameters (a) D, (b) H, (c) OP, (d) IP.

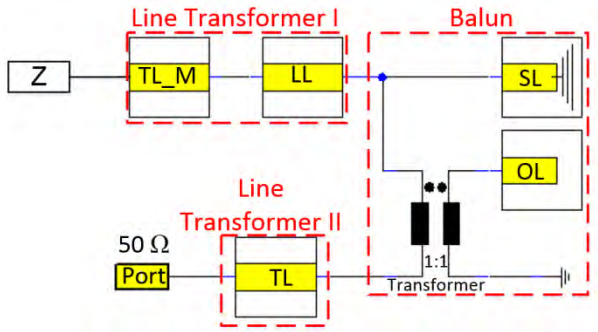

FIGURE 10. Configuration of the matching circuit.

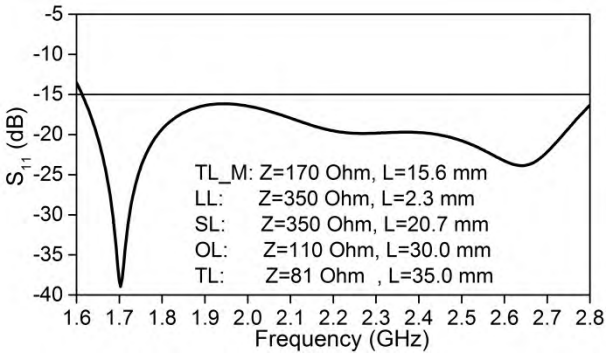

FIGURE 11. Calculated $|S_{11}|$ of the matching circuit model.

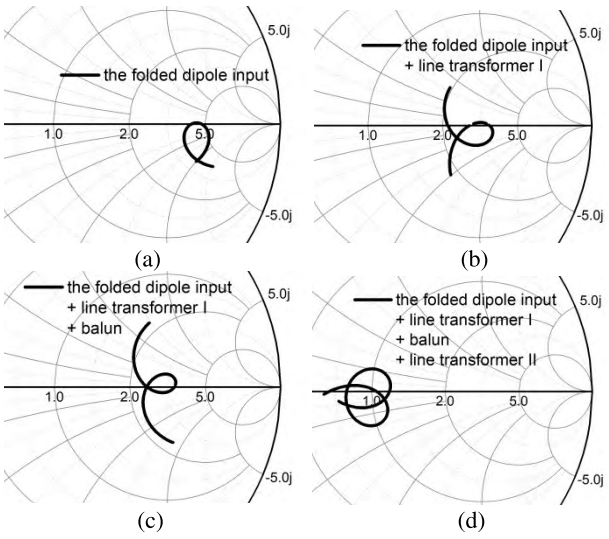

FIGURE 12. Impedance of (a) the folded dipole input, (b) the folded dipole input and the line transformer I, (c) the folded dipole input, line transformer I, and balun, (d) the folded dipole input, the line transformer I, balun, and line transformer II on the Smith chart from 1.60GHz to 2.80 GHz.

$IP = L_5 + 2 \times L_6 + 2 \times L_7$. The variation of input impedance of the folded dipole elements (Z) with different parameter values were studied and shown in Fig. 9. As shown in Fig. 9(a), when the folded dipoles are closely arranged with a small gap, there is a 'fish' pattern indicating a double resonance; but with a wider gap, the resonance disappears. It suggests that the coupling between the folded dipoles plays an importance role in the impedance matching. In this work we choose $G =$ 0.64 mm to get the double resonance. Fig. 9(b) shows that the 'fish' pattern is smaller with a larger H, which indicates a smaller variation of the resistance and reactance across the band, making it easier to be matched. However, low-profile structure is preferred to reduce the mutual coupling between elements when the antenna is applied in an array. Therefore, $H = 27$ mm was chosen as a compromise. Fig. 9(c) and (d) shows the input impedance with different outer and inner perimeters of the folded dipole. Note that when we changing these two parameters, all the related parameters (L_1 to L_7) were scaling up or down together to keep the shape unchanged. It is observed that by changing the outer

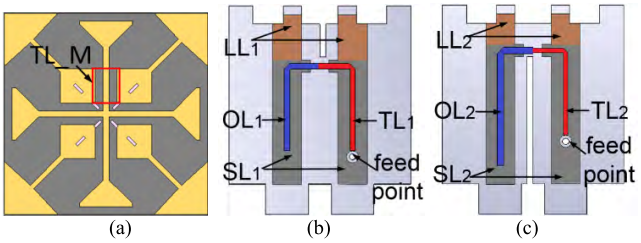

FIGURE 13. Realization of the matching circuit. (a) Top view of antenna aperture, and perspective views of the feed network for (b) +45° polarization, and (c) −45° polarization.

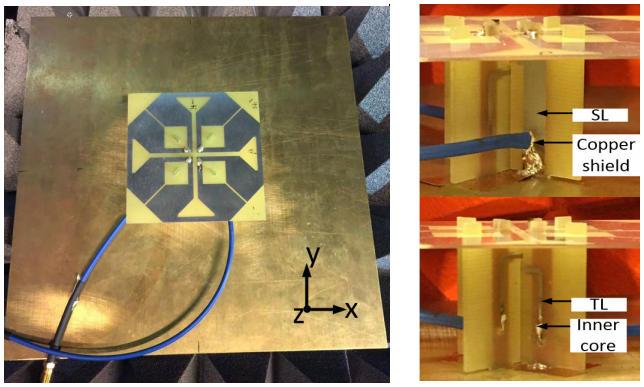

FIGURE 14. (a) Front view and (b) side view of the prototype of the proposed antenna.

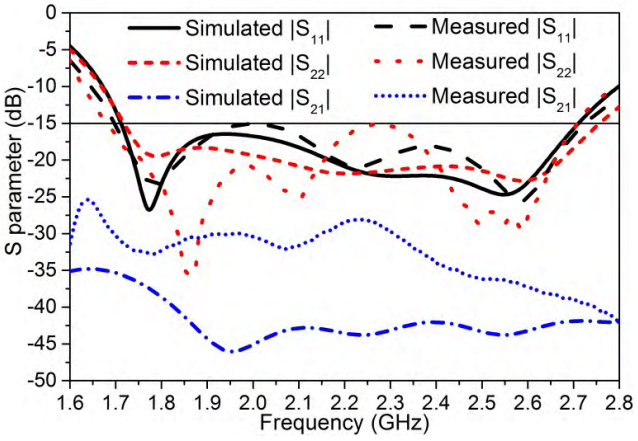

FIGURE 15. Simulated and measured S-parameters.

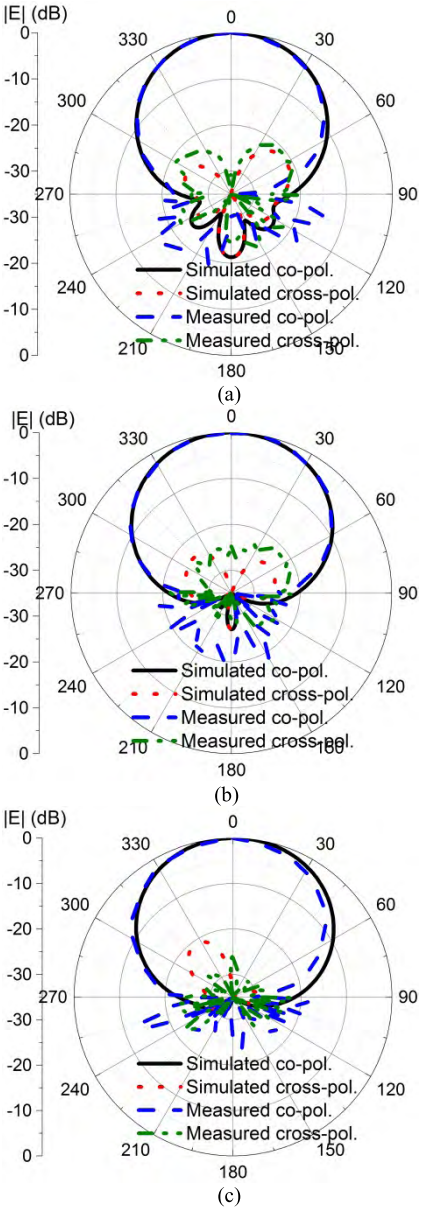

FIGURE 16. Simulated and measured radiation patterns in the horizontal plane at (a) 1.7 GHz, (b) 2.2 GHz, and (c) 2.7 GHz.

perimeter, the resonance moves to higher or lower frequency. The inner perimeter only has influence on the impedance near the starting frequency point (1.7 GHz) while the impedance near the ending frequency point (2.7 GHz) remains stable.

After optimizing the dimension of the folded dipoles and connecting them using parallel conductor transmission lines to the feed points AB and CD, two feed structures are connected to AB and CD to excite the ±45° -polarized radiation separately. In developing the matching circuit, the transmission lines are considered as circuit elements as suggested in [22] and the interaction with the dipole fields is neglected.

The locus of the impedance of the optimized folded dipoles Z on the Smith chart is shown as black solid line in Fig. 9. It shows the characteristic 'fish' pattern indicating a double resonance slightly below the real axis and with a resistive component of approximately 230 Ohms. The task of matching this to 50 Ohms is relatively simple and can be notionally achieved with a wide band two-section transformer that transforms the 230 Ohms to 50 Ohms with some minor reactive corrections.

Fig. 10 shows a circuit representation of the elements involved in the matching. The two-section transformer (line transformer I and II) is formed by transmission lines TL_M, LL, and TL. The balun consisting of short line (SL), open line (OL), and the 1:1 transformer is relatively wideband and does not contribute very much to the matching, however, its components were included in the optimization. The 1:1 transformer is a circuit artifice for connecting the impedance of the OL in series with the impedance of the parallel connection

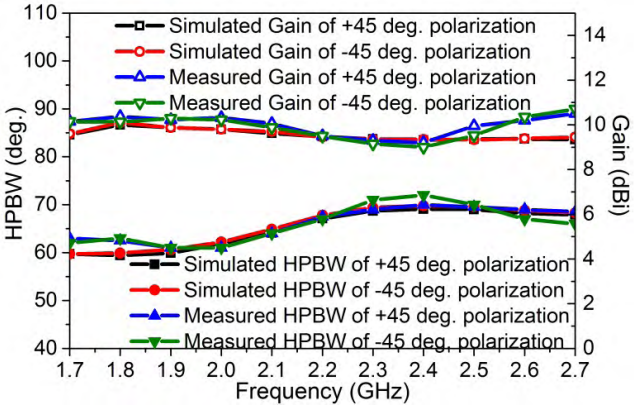

FIGURE 17. Simulated and measured HPBWs and gains.

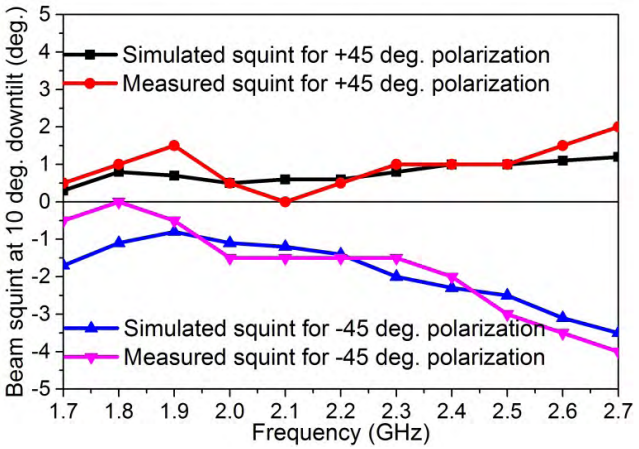

FIGURE 18. Simulated and measured beam squint at 10° down-tilt.

of LL and SL. The optimized parameter values of the circuit elements and the resultant calculated reflection coefficient are shown in Fig. 11. An excellent matching result was obtained with $|S_{11}| < -15$ dB from 1.62 GHz to 2.8 GHz.

To provide insights of how this matching circuit works, the input impedance on Z-Smith Chart with different parts of the matching circuit added are shown in Fig. 12. Fig. 12(a) shows the input impedance of the optimized folded dipoles, which has a double resonance. By adding line transformer I, a third resonance is introduced, and the high resistance of the folded dipole is reduced to some extent, as shown in Fig. 12(b). The balun consisting of SL and OL has minor effect on the impedance, as shown in Fig. 12(c), but they are essential to provide balance feeding. Finally, by employing line transformer II, the input impedance is transformed to around 50 Ohms with a four resonator match, as shown in Fig. 12(d). With this matching circuit, excellent matching (VSWR<1.5) can be realized across the required band.

The implementation of the matching circuit using microstrip technology is shown in Fig. 13. The line TL_M is the parallel conductor line from the folded dipole to the connection points at the center of the PCB. The line LL is a parallel conductor line on the balun board. The component TL and OL are microstrip lines on the balun board. Note that the lines TL_M, LL, and SL are balanced twin conductor

TABLE 2. Optimized parameters for the physical implementation of the matching network.

Elements	Line length (mm)	Line width (mm)	Gap width(mm)
TL_M	14.7	2.7	2.1
LL_1	6.5	4.8	6.0
SL_1	20.5	4.8	6.0
TL_1	18.5	0.9	-
OL_1	18.4	1.0	-
LL_2	4.5	4.8	6.0
SL_2	22.5	4.8	6.0
TL_2	18.6	0.8	-
OL_2	23.3	1.1	-

lines whereas lines OL and TL are unbalanced microstrip lines. The TL and OL are printed on the front layer, whereas LL and SL are printed on the back layer of the substrate. The parameters for these lines are calculated based on the optimized parameters of the corresponding circuit elements. Minor adjustments were made to the layout to optimize the performance with allowance for parasitic discrepancies and the effects of interaction of the circuit components with the dipole fields. Note that the two feed structures are slightly different to avoid interference between the cross-over conductors. The optimized parameters are all listed in Table 2.

V. SIMULATION AND MEASUREMENT RESULTS

The prototype with a 200 × 200 mm^2 ground plane was fabricated and tested, as shown in Fig. 14. Fig. 14(b) illustrates the details of the feed structure. The cables are directly inserted to the feed points (depicted in Fig. 13) with the outer conductor soldered on SL and the inner conductor soldered on TL, as shown in Fig. 14(b). Fig. 15 plots the simulated and measured S-parameters of the two ports. The measured bandwidth for $|S_{11}|/|S_{22}| \leq -15$ dB is 46.4% from 1.69 GHz to 2.71 GHz, which covers the required bandwidth from 1.71 to 2.69 GHz for base station application. The simulated port-to-port isolation is >35 dB and the measured result is around 30 dB over the entire operation frequency band. The simulated and measured radiation patterns at 1.7, 2.2, and 2.7 GHz in the *xoz*-plane are shown in Fig. 16. Only the results of +45° polarization are shown here as antenna is symmetrically arranged and the radiation patterns of the two polarizations are very similar. The simulated and measured patterns agree well. The measured XPD is >25 dB at the main lobe in the horizontal plane. The simulated and the measured front-to-back ratio is >22 dB and >20 dB, respectively. Fig. 17 shows the simulated and measured HPBWs of the antenna for both the two polarizations. The simulated HPBWs are 64.5° ± 5.0° for both two polarizations, and the measured HPBWs are 65.5° ±4.5° and 66.5° ± 5.5° for the +45° and −45° polarization patterns, respectively. The measured results demonstrate that this antenna has very stable radiation patterns across a wide bandwidth. Less beamwidth variation (±3°) is predicted with a ground plane width of 170 mm. The simulated and measured gains are also shown in Fig. 17. The simulated gain varies from 9.3 dBi to 10.1 dBi,

TABLE 3. Comparison of antenna performances.

Antenna type	Ref	Radiator size	Antenna height	Bandwidth	Isolation	HPBW	Shaped reflector	Gain	XPD	Squint
Type-I Cross-dipole	[3]	$0.39\lambda_0$*$0.39\lambda_0$	$0.27\lambda_0$	54.5% ($\|S_{11}\|$<−14 dB)	>28.5 dB	66.2° ± 3.7°	Yes	8.5 ± 0.9 dBi	NG	NG
	[7]	$0.41\lambda_0$*$0.41\lambda_0$	$0.25\lambda_0$	45% ($\|S_{11}\|$<−15 dB)	> 25 dB	68° ± 2°	Yes	8.2 ± 0.6 dBi	NG	NG
	[8]	$0.45\lambda_0$*$0.45\lambda_0$	$0.23\lambda_0$	48% ($\|S_{11}\|$<−15 dB)	> 22 dB	62° ± 4°	Yes	8.2 ± NG dBi	19 dB	NG
Type-II ME-dipole	[14]	$0.49\lambda_0$*$0.49\lambda_0$	$0.15\lambda_0$	24.9% ($\|S_{11}\|$<−10 dB)	> 29 dB	60.5° ± 1.5°	No	8.2 ± NG dBi	NG	NG
	[15]	$0.45\lambda_0$*$0.45\lambda_0$	$0.25\lambda_0$	48.0% ($\|S_{11}\|$<−14 dB)	> 30 dB	67.1 ± 10°	Yes	8.5 ± 0.9 dBi	21 dB	NG
Type III Square dipole array	[18]	$0.49\lambda_0$*$0.49\lambda_0$	$0.23\lambda_0$	23.7% ($\|S_{11}\|$<−14 dB)	> 30 dB	65.3° ± 1.2°	Yes	9.7 ± 0.2 dBi	23.5 dB	NG
	[19]	$0.42\lambda_0$*$0.42\lambda_0$	$0.23\lambda_0$	27.8% ($\|S_{11}\|$<−14 dB)	> 25 dB	65° ± 5°	No	8.0 ± NG dBi	16 dB	NG
	This work	$0.51\lambda_0$*$0.51\lambda_0$	$0.20\lambda_0$	46.4% ($\|S_{11}\|$<−15 dB)	> 28 dB	66.5° ± 5.5°	No	9.8 ± 0.9 dBi	25 dB	< 4°

and the measured gain varies from 9.0 dBi to 10.7 dBi within the targeted bandwidth. The radiation efficiency is above 80% across the operating frequency band. The beam squint results are shown in Fig. 18. At 10° down-tilt, the simulated and measured beam squints are all <4°.

In addition, a detailed comparison between the proposed antenna element and other types of base station antenna elements reported in recently published literatures is provided in Table 3. It can be seen from the table that, using a well-designed type-III structure, the antenna element achieves comparable performances to that of type-I cross-dipole, but it does not need additional modifications on the ground plane, thus being more suitable to be used in a base station antenna array. Compared with type-II ME-dipole, the proposed antenna element has stable radiation patterns across a wider well-matched band. Compared with other type-III antennas, the bandwidth of the antenna is almost doubled. Moreover, reduced beam squint <4° is achieved in this work. Although the aperture size is slightly larger than other published work, the profile is reduced to $0.20\lambda_0$, which can help to reduce mutual coupling when the element is used in an antenna array. The comparison demonstrates that the proposed antenna element is a competitive candidate for base station applications.

VI. CONCLUSION

A wideband ±45° dual-polarized antenna element comprising four simultaneously excited folded dipoles is proposed for base station applications. The antenna features excellent radiation performance including wide bandwidth, high port-to-port isolation, low cross polarization, stable radiation patterns, and reduced beam squint. The element requires no walls or other external beam shaping and is ideal for use in dual band antenna systems. Moreover, the theoretical analysis of the radiation properties of the antenna element and the circuit theory model of the feed network provide a valuable guidance for the general design of current and future base station antennas.

REFERENCES

[1] Y. Liu, H. Yi, F.-W. Wang, and S.-X. Gong, "A novel miniaturized broadband dual-polarized dipole antenna for base station," *IEEE Antennas Wireless Propag. Lett.*, vol. 12, pp. 1335–1338, 2013.
[2] D.-Z. Zheng and Q.-X. Chu, "A multimode wideband ±45° dual-polarized antenna with embedded loops," *IEEE Antennas Wireless Propag. Lett.*, vol. 16, pp. 633–636, 2017.
[3] D.-Z. Zheng and Q.-X. Chu, "A wideband dual-polarized antenna with two independently controllable resonant modes and its array for base-station applications," *IEEE Antennas Wireless Propag. Lett.*, vol. 16, pp. 2014–2017, 2017.
[4] Y. Gou, S. Yang, J. Li, and Z. Nie, "A compact dual-polarized printed dipole antenna with high isolation for wideband base station applications," *IEEE Trans. Antennas Propag.*, vol. 62, no. 8, pp. 4392–4395, Aug. 2014.
[5] Z. Bao, Z. Nie, and X. Zong, "A novel broadband dual-polarization antenna utilizing strong mutual coupling," *IEEE Trans. Antennas Propag.*, vol. 62, no. 1, pp. 450–454, Jan. 2014.
[6] Y. Cui, R. Li, and H. Fu, "A broadband dual-polarized planar antenna for 2G/3G/LTE base stations," *IEEE Trans. Antennas Propag.*, vol. 62, no. 9, pp. 4836–4840, Sep. 2014.
[7] Q.-X. Chu, D.-L. Wen, and Y. Luo, "A broadband ±45° dual-polarized antenna with Y-shaped feeding lines," *IEEE Trans. Antennas Propag.*, vol. 63, no. 2, pp. 483–490, Feb. 2015.
[8] H. Huang, Y. Liu, and S. Gong, "A broadband dual-polarized base station antenna with sturdy construction," *IEEE Antennas Wireless Propag. Lett.*, vol. 16, pp. 665–668, 2017.
[9] H. Huang, Y. Liu, and S. Gong, "A novel dual-broadband and dual-polarized antenna for 2G/3G/LTE base stations," *IEEE Trans. Antennas Propag.*, vol. 64, no. 9, pp. 4113–4118, Sep. 2016.
[10] H. Huang, Y. Liu, and S. Gong, "A dual-broadband, dual-polarized base station antenna for 2G/3G/4G applications," *IEEE Antennas Wireless Propag. Lett.*, vol. 16, pp. 1111–1114, 2017.
[11] Y. He, W. Tian, and L. Zhang, "A novel dual-broadband dual-polarized electrical downtilt base station antenna for 2G/3G applications," *IEEE Access*, vol. 5, pp. 15241–15249, Jun. 2017.
[12] H. Huang, Y. Liu, and S. Gong, "A broadband dual-polarized base station antenna with anti-interference capability," *IEEE Antennas Wireless Propag. Lett.*, vol. 16, pp. 613–616, 2017.
[13] K. M. Luk and H. Wong, "A new wideband unidirectional antenna element," *Int. J. Microw. Opt. Technol*, vol. 1, pp. 35–44, Apr. 2006.
[14] L. Siu, H. Wong, and K. M. Luk, "A dual-polarized magneto-electric dipole with dielectric loading," *IEEE Trans. Antennas Propag.*, vol. 57, no. 3, pp. 616–623, Mar. 2009.

[15] M. Li and K.-M. Luk, "Wideband magnetoelectric dipole antennas with dual polarization and circular polarization," *IEEE Antennas Propag. Mag.*, vol. 57, no. 1, pp. 110–119, Feb. 2015.
[16] T. Ai, "Bipolarized antenna," CN Patent 100 461 530 C, Feb. 11, 2009.
[17] R. Gabriel and M. Gottl, "Dual-polarized dipole antenna," U.S. Patent 6 313 809 B1, Nov. 6, 2001.
[18] Y.-H. Huang, Q. Wu, and Q.-Z. Liu, "Broadband dual-polarised antenna with high isolation for wireless communication," *Electron. Lett.*, vol. 45, no. 14, pp. 714–715, Jul. 2009.
[19] D.-L. Wen, D.-Z. Zheng, and Q.-X. Chu, "A dual-polarized planar antenna using four folded dipoles and its array for base stations," *IEEE Trans. Antennas Propag.*, vol. 64, no. 12, pp. 5536–5542, Dec. 2016.
[20] S.-G. Zhou, P.-K. Tan, and T.-H. Chio, "Low-profile, wideband dual-polarized antenna with high isolation and low cross polarization," *IEEE Antennas Wireless Propag. Lett.*, vol. 11, pp. 1032–1035, 2012.
[21] R. F. Harrington, "Introduction to waves," in *Time-Harmonic Electromagnetic Fields*. New York, NY, USA: Wiley, 2001, p. 82.
[22] C. Ding, B. Jones, Y. J. Guo, and P.-Y. Qin, "Wideband matching of full-wavelength dipole with reflector for base station," *IEEE Trans. Antennas Propag.*, vol. 65, no. 10, pp. 5571–5576, Oct. 2017.

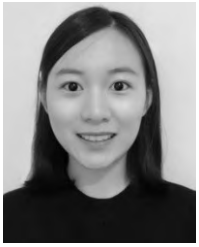

HAIHAN SUN (GS'17) was born in Shandong, China, in 1994. She received the bachelor's degree in electronic information engineering from the Beijing University of Posts and Telecommunications, Beijing, China, in 2015. She is currently pursuing the Ph.D. degree in engineering at the University of Technology Sydney, Sydney, Australia.

Her current research interests include base station antennas and wideband omnidirectional antennas.

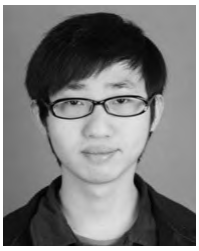

CAN DING (M'17) was born in Anhui, China, in 1989. He received the bachelor's degree in micro-electronics from Xidian University, Xi'an, China, in 2009, and the Ph.D. degree from Macquarie University, Sydney, Australia, in 2015. From 2012 to 2015, he was under the Cotutelle agreement between Macquarie University, Australia, and Xidian University, China. During this period, he was also with the Commonwealth Scientific and Industrial Research Organisation, DPaS Flagship, Marsfield, Australia. From 2015 to 2017, he was a Post-Doctoral Research Fellow with the University of Technology Sydney, Sydney, Australia. He is currently a Lecturer with the Global Big Data Technologies Centre, University of Technology Sydney, Sydney, Australia. His research interest is in the area of reconfigurable antenna, phase shifter, and base station antenna.

BEVAN JONES (LM'13) was born and educated in Sydney, Australia. He received the B.Sc., B.E. (Hons.), and the Ph.D. degree from the University of Sydney, Australia, in 1967, 1970, and 1974, respectively, all in electrical engineering.

From 1974 to 1977, he was a Post-Doctoral Fellow with the Max-Planck-Institut für Radioastronomie, Bonn, Germany, where he was involved in the design of a millimeter wavelength radiotelescope. He was a Lecturer with Wollongong University, Australia, for two years. He then returned to Germany as a Scientist. In 1980, he returned to Australia to work on the Interscan Project to develop a microwave aircraft landing system (MLS). From 1980 to 1982, he led a group of twelve Australian engineers involved in this project in USA with a joint venture partner.

From 1983 to 1994, he was the Technical Director of Interscan Australia Pty Ltd., an R&D company owned and funded by the Australian Industry Development Corporation. He led the development of many antenna based products including the microwave landing system, a C-band phased array precision approach system, an electronically scanned TACAN navigation beacon, a large vertical aperture secondary surveillance radar antenna, and an advanced S-band multi-beam phased array primary radar antenna. From 1992 to 1993, he was also responsible for the development of early cellular base station antennas, the first with adjustable electrical beam tilt at the time when the original AMPS system was being rolled out. In 1994, together with two partners, he founded Argus Technologies, Australia, and served as the Managing Director for ten years and then as the Technical Director. The company has specialized solely in the design and manufacture of cellular base station antennas and expanded its market reach worldwide. The company initially operated at Sydney but set up a second manufacturing facility in Guangzhou, China, in 2001, and later established an R&D capability. Since its inception, Argus has brought many innovations to market and became a major international supplier of cellular antennas. In 2011, the company was acquired by a U.S. multinational, where he served as the Technical Director under the new ownership for two years, during which he was largely engaged in technical instruction of the group's engineering teams in the U.S. and China. Following that he retired from full-time work and since then has done a number of consulting jobs on antenna related topics. He is currently an Adjunct Professor with the University of Technology Sydney. He has authored a number of articles in technical journals and patents relating to antenna components and has done consulting on antennas and electromagnetics for a number of companies including Raytheon and British Aerospace and has taught specialist courses in numerical methods and electromagnetics at universities.

Y. JAY GUO (F'14) received the B.S. and the B.S. degrees from Xidian University, China, in 1982 and 1984, respectively, and the Ph.D. degree from Xian Jiaotong University, China, in 1987.

He held various senior leadership positions in Fujitsu, Siemens, and NEC in the U.K. He served as the Director of CSIRO for over nine years, where he was involved in directing a number of ICT research portfolios. He is currently a Distinguished Professor and the founding Director of the Global Big Data Technologies Centre, University of Technology Sydney, Australia. He has authored over 300 research papers and holds 22 patents in antennas and wireless systems. His research interest includes antennas, mm-wave and THz communications, sensing systems, and big data.

Prof. Guo is a fellow of the Australian Academy of Engineering and Technology and the IET, and a member of the College of Experts of Australian Research Council. He has received a number of most prestigious Australian national awards, and was named one of the most influential engineers in Australia in 2014 and 2015, respectively. He has chaired numerous international conferences. He was the International Advisory Committee Chair of the IEEE VTC2017, the General Chair of ISAP2015, iWAT2014, and WPMC'2014, and the TPC Chair of the 2010 IEEE WCNC, and the 2012 and 2007 IEEE ISCIT. He served as a Guest Editor of special issues on 'Antennas for Satellite Communications and Antennas and Propagation Aspects of 60-90GHz Wireless Communications, both in the IEEE TRANSACTIONS ON ANTENNAS AND PROPAGATION, Special Issue on Communications Challenges and Dynamics for Unmanned Autonomous Vehicles, the IEEE JOURNAL ON SELECTED AREAS IN COMMUNICATIONS, and Special Issue on 5G for Mission Critical Machine Communications, the *IEEE Network Magazine*.